# Eccentric Virtual Array Source Aperture (EVASA)—Ultrasound Imaging Technique Using Phased Array Excitation

THACKER SETU RAMESHBHAI, THULSIRAM GANATALA and KRISHANAN BALASUBRAMANIAN

## ABSTRACT

The traditional phased array ultrasound technique (PAUT) uses active focusing of elements to achieve beam forming and improved imaging capabilities. The recent approach involving FMC/TFM improves this method using synthetic reconstruction approaches. In this research, we introduce a novel hybrid approach that combines active and synthetic focusing at specific angle configurations, utilizing an Eccentric Virtual Array of Source Aperture (EVASA) in the Phased Array Ultrasonic Testing (PAUT) method. Some of the key advantages of this EVASA approach include (a) transmission at a specific angle with focus at a certain depth (b) lower time for inspection, (c) improved imaging of defect shapes and sizes, and (d) improved imaging of defects in regions where it was hard to reach (e) inspect the defects in much thicker samples with ease compared to FMC/TFM. The EVASA method employs a custom algorithm where array elements transmit ultrasound waves with pre-calculated delay laws, achieving beamforming focused at eccentric virtual sources located beneath the transducer. These virtual sources will focus on particular depths and angles, which will send a high-amplitude wave into the material for inspection at much deeper defects. Once the desired set of eccentric virtual sources has been formed within the material, the synthetic algorithms of FMC/TFM can be used to image the regions of inspection into the material. The parameters for forming the virtual sources, including their number, aperture position in the probe, and coordinates within the material, are based on the propagation angle and focal depth, extending up to the near-field distance. Comparative evaluation of EVASA with FMC/TFM shows its significant advantages, using metrics like Signal-to-Noise Ratio (SNR) which show substantial improvements. Importantly, EVASA is implemented using standard PAUT probes and instruments, requiring only customization in focal laws and reconstruction algorithms.

## INTRODUCTION

Non-destructive evaluation (NDE) ultrasound imaging is being used in many sectors,

Thacker Setu Rameshbhai, MS Student, Email: me23s027@smail.iitm.ac.in. Centre for Non-Destructive Evaluation (CNDE), Machine Design Section, Mechanical Engineering Department, Indian Institute of Technology Madras, Chennai, India

including energy, oil and gas, manufacturing, aerospace, and defense, to inspect various structures to prevent sudden breakdown of machinery [1]. In NDE, Ultrasonic Testing (UT) is one of the safest and fastest methods compared to Radiography, Computer Tomography (CT), Induction thermography, Eddy current testing, etc. These inspection methods help to characterize defects in a much more accurate and precise way at the manufacturing stage and even in in-service applications. These defects can grow while in-service till a certain length, after that these defects can cause catastrophic failure, and a hazardous incident can occur. So, it is very necessary to examine a large critical structure at a faster pace to reduce downtime and cost.

In UT, the use of ultrasound phased array transducers becomes quite normal to perform faster inspection compared to using a conventional UT probe with a single element [2]. The ultrasonic phased array employs multiple single-element transducers, which can be individually excited with specific delays [3]. It can generate a TFM image, which helps to characterize the defect in a more efficient way to maintain the structural integrity of the large critical components, like boilers, nuclear, oil, and gas pipelines, thick weld joints, etc.

Ultrasound Phased Array (PA) technology enables beam focusing and beam steering within a material, allowing for faster inspection and more coverage due to simultaneous excitation of multiple elements in the aperture. A-Scans must be processed and converted into TFM images to analyze the acquired data from the Phased Array. Total Focusing Method (TFM) is an advanced imaging technique that significantly enhances image resolution and defect characterization [4]. TFM works as if it focuses on each pixel in the region of interest (ROI), which is called synthetic focusing, which is not a real focusing. TFM is a postprocessing method that works on top of Full Matrix Capture (FMC), where each element is sequentially excited and receives the reflected signal from every element present in the probe. Mainly, Full Matrix Capture (FMC) is one of the data collection methods. That offers flexibility and allow users to tailor acquisition settings based on specific inspection needs. TFM image is having better signal-to-noise ratio (SNR) for defect detection. However, TFM algorithms is computationally heavy because they can't be used for real-time inspection. Moreover, it uses only single element excitation, which can't travel far enough, that's makes it useless to inspect thicker samples. On top of it, the signal-to-noise ratio (SNR) of thicker samples is quite low because of the firing of a single element at a time.

To overcome the limitations of low transmitting energy and reduced signal-to-noise ratio (SNR), the group of elements can be excited simultaneously with specific delay laws, generating a focused beam at a specific location inside the material. At this location, the wavefronts from all active elements constructively interfere, resulting in a higher-energy wavefront. This enhanced wavefront can penetrate deeper into the material with reduced attenuation, enabling the inspection of thicker samples. This predefined focal point is referred to as a Virtual Source (VS) because it acts as an internal excitation point within the material, effectively functioning as a secondary source of ultrasonic waves [5]. The placement of Virtual Sources can be strategically determined using specific patterns to optimize inspection performance, enhance imaging resolution, and achieve specific evaluation objectives.

## METHODOLOGY

### Full Matrix Capture (FMC)

Full Matrix Capture (FMC) is a data collection method that is widely used in Non-Destructive Testing (NDT), specifically in Ultrasonic Testing (UT). In this technique, every element of the transducer is excited sequentially, and the signal is captured by all the elements [6]. When the $i^{th}$ element exited and that wavefront propagated into the material. After reflecting from the reflector, the signal of this wavefront is received by all the elements. The signal is captured by one element called A-Scan. This process keeps happening till each element is excited once, sequentially. If there are N elements in the transducer, then there will be an "N x N" matrix of A-Scans. These signals are stored in the FMC matrix $A_{ij}(t)$, whose dimensions would be "N x N x time". Because each A-scan would have information about reflectors present inside the material. To accurately locate the position of the reflector, it is necessary to include the time component of the A-scan signals.

FMC stores a lot of data that helps to generate a high-resolution image. By having a large amount of data, the inspector can perform various post-processing techniques to enhance the Signal-to-noise ratio (SNR).

### Total Focusing Method (TFM)

Total Focusing Method (TFM) is a post-processing method that uses data collected via Full Matrix Capture (FMC). TFM is an advanced image reconstruction algorithm in which the region of interest (ROI) is subdivided into multiple pixels using grids. TFM synthetically (virtually) focused on each pixel in the region of interest (ROI) in the x-z plane. To virtually focus on each pixel, the ultrasonic beam needs to adjust focal depth (F) and steering angle (theta). In Fig. 1, it represents the transmitting and receiving elements are represented as "t" and "r", respectively. The time delay corresponding to the pixel is the sum of the time travel from transmitting element $(x_t, z_t)$ to the pixel $(x_p, z_p)$ and from that pixel to receiving element $(x_r, z_r)$. To define the intensity $I_1(x, z)$ at the point of the pixel $(x_p, z_p)$, it requires summing up the amplitude of all the signals in the time domain (A-scans) from the FMC matrix as per Eq. 1. By just using A-scan data $(A_{ij})$, the generated TFM image contains a lot of artifacts. To reduce these artifacts in the generated TFM image, by introducing the imaginary part of the Hilbert transform of A-scan data $(A_{ij})$, which is defined at $M_{ij}$ can be resolved as per Eq. 2. To reconstruct the TFM image, the process of delay-sum needs to be performed for all the pixel points within the region of interest (ROI) [4].

$$I_1(p) = \left| \sum_{i=1}^{N} \sum_{j=1}^{N} A_{ij} \left( t_i^p + t_j^p \right) \right| \tag{1}$$

$$I_2(p) = \left| \sum_{i=1}^{N} \sum_{j=1}^{N} A_{ij} \left( t_i^p + t_j^p \right) + \sum_{i=1}^{N} \sum_{j=1}^{N} M_{ij} \left( t_i^p + t_j^p \right) \right| \tag{2}$$

here,

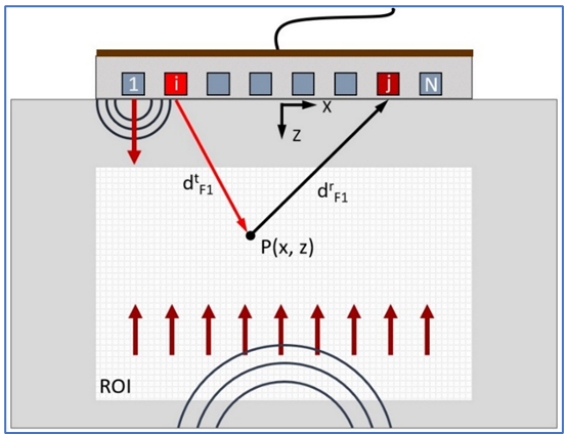


Figure 1. TFM image

$$t_i^p = \frac{\sqrt{(x_t - x_p)^2 + z_p^2}}{C_i^{(t)}} \tag{3}$$

$$t_j^p = \frac{\sqrt{(x_p - x_r)^2 + z_p^2}}{C_j^{(r)}} \tag{4}$$

$t_i^p$, $t_j^p$, $C$, and $I_2(p)$ are the delay time from transmitting element to pixel point, delay time from pixel point to receiving element, the velocity of sound inside the material, and Intensity matrix, respectively.

**Virtual Aperture Source Array (VASA)**

Virtual Array Source Aperture (VASA) is the technique that excites many elements (4,8,16, and 32) with predefined focal laws to create a converging beamform at a specific point inside the material. That point is called a virtual source, which behaves exactly like a source but is not a real one [7]. This virtual source's location can impact the TFM image's SNR. In VASA, we have chosen the location of the virtual source at the centre of the active aperture and a specific depth from the top surface.

The concept of VASA is to excite multiple elements rather than to excite a single element at a time in FMC. If the total number of elements available in the probe is N, then the total transmission would be N and $N - n + 1$ in FMC and VASA, respectively. Where n is the number of active elements in the aperture [8] [9] [10].

In FMC, the generated wavefront was not able to travel at a much deeper distance, but by introducing the concept of a virtual source, multiple wavefronts focus at a specific point, and an energized wavefront starts to propagate into the material from that virtual source. Once this higher energized wavefront is reflected from the reflector, A-scans will be recorded by all the elements and form an FMC matrix. This will help to find the intensity $I_{VASA}(p)$ of every pixel $p(x, z)$ in the region of interest in the reconstructed TFM image using the following Eq. 5

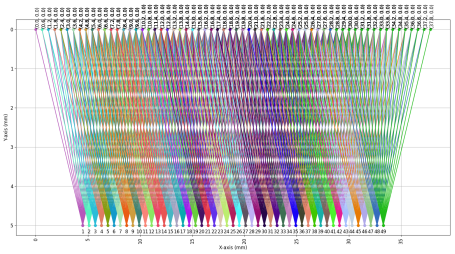

Figure 2. Virtual sources of VASA

$$I_{VASA}(p) = \sum_{i=1}^{N_v} \sum_{j=1}^{N_e} A_{ij} \left( t_i^p + t_j^p + \tau_{vs}^{\max} \right) + \sum_{i=1}^{N_v} \sum_{j=1}^{N_e} M_{ij} \left( t_i^p + t_j^p + \tau_{vs}^{\max} \right) \tag{5}$$

Here, $\tau_{vs}$ denotes the time required for the wave to travel from the virtual source to the elements within the active aperture. Hence, $\tau_{vs}^{max}$ is added in Eq. 5, because the wave is transmitted from $1^{st}$ element of active aperture in any transmission.

$$\tau_{vs} = \frac{d_{D_i}^{(t)}}{C_i^{(t)}} = \frac{\sqrt{(x_i - x_v)^2 + z_v^2}}{C_i^{(t)}} \tag{6}$$

$N_v$ represents the count of virtual sources, while $N_e$ denotes the number of elements within the transducer. While $t_i^p$ and $t_j^p$ are the travelling time from the virtual source to any pixel in the ROI, and from that same pixel to the receiving element in the transducer, respectively.

## EVASA-TFM

In FMC and VASA, wavefronts travel straight into the materials using synthetic focusing and beam focusing, respectively. These two methods are working well if the region of interest(ROI) is just below the transducer. But, if the region of interest is away from the transducer, then it's difficult for FMC and VASA to capture the exact shape and size of the reflector available in the sample. To capture these distant reflectors, a change in the location of virtual sources can be impactful in extracting the correct shape and size of the reflector. The primary challenge currently lies in determining optimal virtual source configurations to direct waves at specific angles without relying on angle wedges.

In this study, we propose a novel method termed Eccentric Virtual Array Source Aperture (EVASA). In EVASA, multiple elements are being used as an active aperture with predefined delay laws to send a higher energised wavefront at a specific angle after focusing at a specific virtual source within the near field region. EVASA introduces the critical capability of steering the wavefront at a desired angle. Which is not available in the original VASA method.

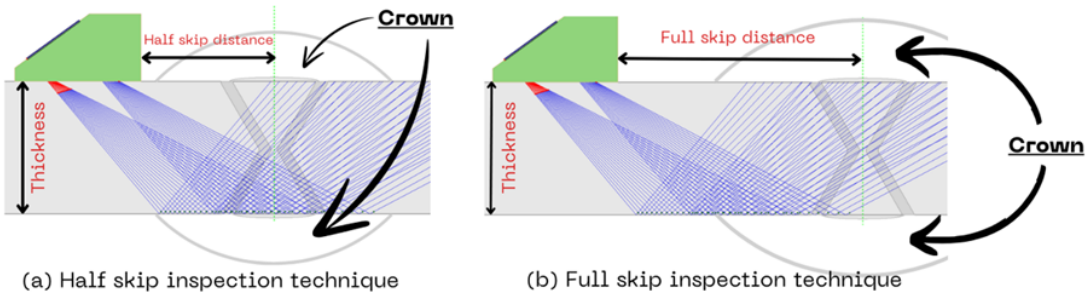


Figure 3. Weld sample having inspection with different skips to cover the entire weld region

It is important to note that when the region of interest (ROI) is just below the transducer, then Full Matrix Capture and Virtual Array Source Aperture will give superior results compared to EVASA. However, in case the region of interest is located at a lateral offset from the transducer, EVASA will dominate the result compared to FMC and VASA due to it's steering capability.

The EVASA method is particularly advantageous for the inspection of welded samples. In conventional Phased Array Ultrasonic Testing (PAUT), operators need to use an angle wedge to cover the entire welded region, which includes root, heat-affected zone (HAZ), top and bottom capping (weld beads), and some part of the base metal, as illustrated in Fig. 3. In contrast, the proposed EVASA method can perform weld inspection without relying on an angle wedge by electronically steering a focused ultrasonic beam at a specified angle within the material. This allows for covering the entire weld region by appropriately placing the virtual sources. To perform EVASA, we need to shift the position of virtual sources by $\theta$ angle using Eq. 7.

$$X_{\text{shift}} = Y_{\text{shift}} \cdot \tan(\theta) \tag{7}$$

$Y_{shift}$ and $\theta$ are independent variables that the user can choose to steer the ultrasonic beam. $Y_{shift}$ can be varied for each transmission; it does not need to be fixed for all transmissions. Based on $Y_{shift}$ and $\theta$, $X_{shift}$ will be derived, and it will be added to the position of the virtual sources in the x-coordinate.

## EXPERIMENTATION AND EVALUATION

### Experimental setup

To demonstrate the steering capability of the novel EVASA method, we utilized a calibration block as shown in Fig. 4.Our experimental setup utilizes an Eddify M2M Panther 32/128 transmitter-receiver flaw detector, integrated with CPU input/output interfaces. The system is paired with a linear phased array probe operating at a central frequency of 5 MHz, comprising 64 elements with a 0.6 mm pitch. The sample, depicted in Fig. 4, is made of mild steel SS316, with a thickness of 49 mm. The holes in the sample have a diameter of 3 mm and are spaced 9.8 mm apart, numbered sequentially from 1 to 4 from top to bottom, respectively.

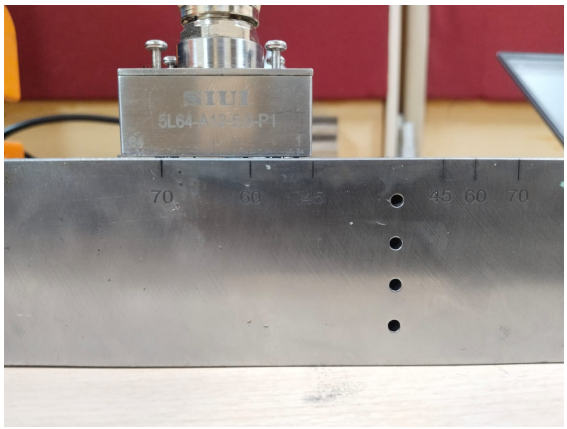

Figure 4. Calibration block

ACQUIRE software was employed to capture the A-scans received from the reflectors. This software enables users to define physical dimensions, specify material properties, configure custom focal laws, set the number of elements in the active aperture, and select transmission–reception element pairs. It also facilitates the precise control of experimental parameters such as the location of virtual sources.

The distance between the transducer's closest edge and the center of each SDH is maintained at 20 mm. With this configuration, FMC, VASA, and EVASA techniques were applied to the sample, enabling a quantitative comparison of the signal-to-noise ratio (SNR).

| **Parameters** | **Value** |
|---|---|
| Number of elements | 64 |
| Element width (mm) | 0.52 |
| Element pitch (mm) | 0.6 |
| Total active length (mm) | 38.4 |
| Center frequency (MHz) | 5 |
| Elevation (mm) | 10 |
| Sampling rate (MHz) | 62.5 |

TABLE I. Specification of phased array probe used in experiment.

## Result and Discussion

We have performed EVASA-TFM on the given sample using various virtual source patterns, as illustrated in Fig. 5 (a-g). Below, we elaborate on the naming convention adopted for the patterns used to generate the TFM images from EVASA data:

- **VASA_F5**: The virtual source is positioned at the center of the active aperture at a depth of 5 mm.
- **EVASA_F5_S30**: The virtual sources are shifted by 30 degrees towards the right at a depth of 5 mm.

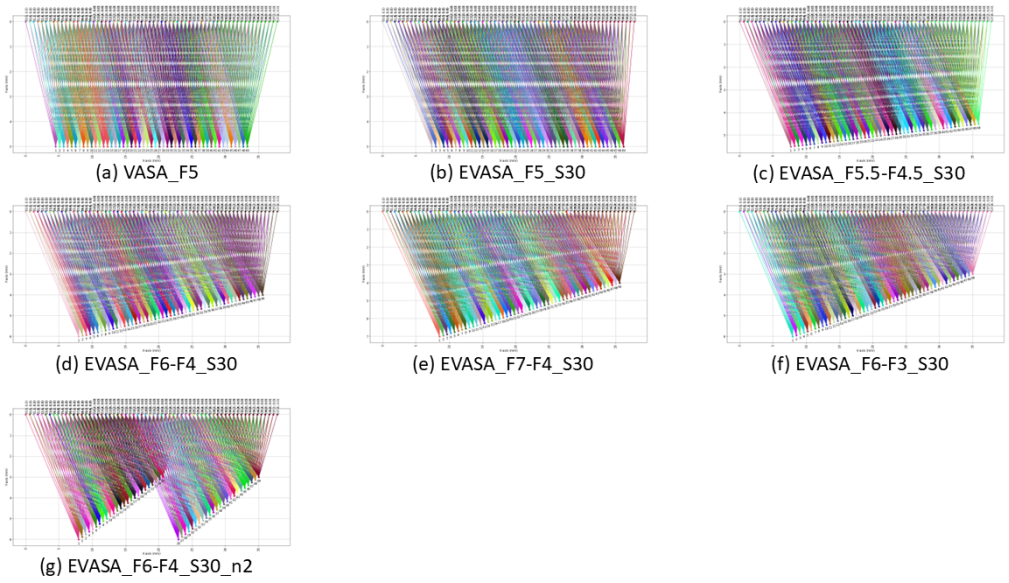


Figure 5. Various cases of selection of virtual sources

- **EVASA_F5.5-F4.5_S30**: The virtual sources are shifted by 30 degrees towards the right, with their depths varying from 5.5 mm to 4.5 mm.
- **EVASA_F6-F4_S30**: The virtual sources are shifted by 30 degrees towards the right, with depths ranging from 6 mm to 4 mm.
- **EVASA_F7-F4_S30**: The virtual sources are shifted by 30 degrees towards the right, with depths ranging from 7 mm to 4 mm.
- **EVASA_F6-F3_S30**: The virtual sources are shifted by 30 degrees towards the right, with depths ranging from 6 mm to 3 mm.
- **EVASA_F6-F4_S30_n2**: The virtual sources are shifted by 30 degrees towards the right, with depths varying from 6 mm to 4 mm, divided into two separate segments.

After generating TFM images using all the above patterns of the virtual source, it indicates the presence of side-drilled holes (SDHs). To quantitatively assess the image quality, the signal-to-noise ratio (SNR), as defined in Eq. 8, was computed for each defect (#1 to #4 from top to bottom) across all variations, as presented in Fig. 6.

$$SNR = 20 * \log_{10} \left| \frac{I_{\max}}{I_{\text{average}}} \right| \tag{8}$$

After comparing the SNR values of all four defects across various virtual source patterns, as shown in Fig. 7, we conclude that pattern (d), **EVASA_F6-F4_S30**, outperforms all other configurations. The SNR values for the side-drilled holes #1 to #4 using this pattern are 26.42 dB, 38.4 dB, 45.86 dB, and 48.85 dB, respectively. This makes **EVASA_F6-F4_S30** one of the most effective configurations for directing waves

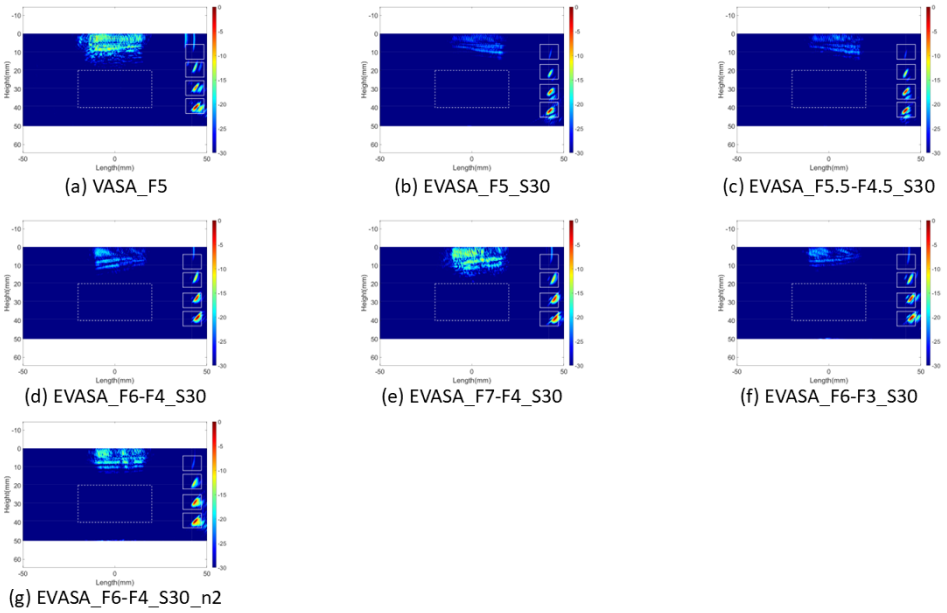


Figure 6. TFM images of Various cases of selection of virtual sources

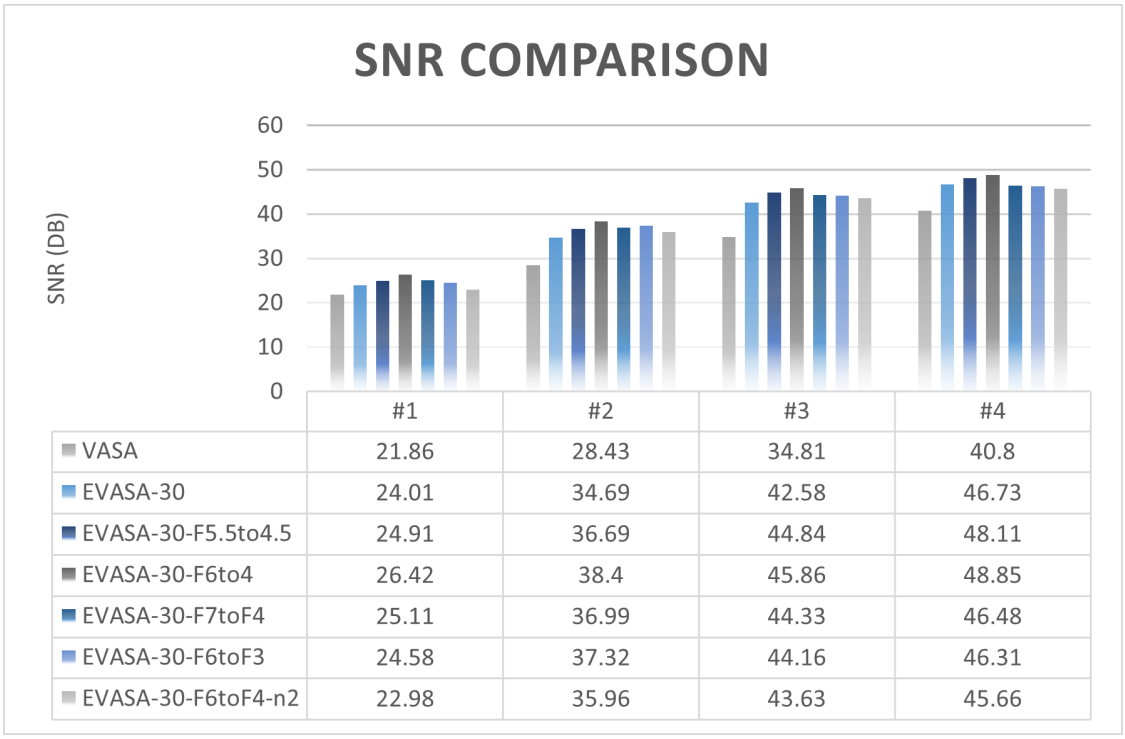


| | #1 | #2 | #3 | #4 |
|---|---|---|---|---|
| VASA | 21.86 | 28.43 | 34.81 | 40.8 |
| EVASA-30 | 24.01 | 34.69 | 42.58 | 46.73 |
| EVASA-30-F5.5to4.5 | 24.91 | 36.69 | 44.84 | 48.11 |
| EVASA-30-F6to4 | 26.42 | 38.4 | 45.86 | 48.85 |
| EVASA-30-F7toF4 | 25.11 | 36.99 | 44.33 | 46.48 |
| EVASA-30-F6toF3 | 24.58 | 37.32 | 44.16 | 46.31 |
| EVASA-30-F6toF4-n2 | 22.98 | 35.96 | 43.63 | 45.66 |

Figure 7. SNR comparisons of all cases of selection of virtual sources

in a specific direction and depth, enabling the clear identification of defects that would otherwise be masked by noise in the surrounding region.

It is evident from Fig. 6 that the positioning pattern of the virtual sources significantly affects the results. This observation suggests that there may be unexplored patterns that could yield better outcomes than those derived in this study.

Future work can focus on systematically optimizing virtual source configurations using advanced search methods like genetic algorithms, machine learning-based approaches, or reward-based approaches like Reinforcement Learning.

## REFERENCES


1. Cruza, J. F., J. Camacho, R. Mateos, and C. Fritsch. 2019. "A new beamforming method and hardware architecture for real time two way dynamic depth focusing," *Ultrasonics*, 99:105965, ISSN 0041-624X, doi:https://doi.org/10.1016/j.ultras.2019.105965.
2. Zhang, Y., X.-R. Gao, C.-Y. Peng, Z. Wang, and X. LI. 2017. "Research on High Speed Phased Array Ultrasonic Inspection System," in *2017 Far East NDT New Technology Application Forum (FENDT)*, pp. 233–236, doi:10.1109/FENDT.2017.8584575.
3. Jr., L. W. S. 2015. *Fundamentals of Ultrasonic Phased Arrays*, vol. 215 of *Solid Mechanics and Its Applications*, Springer, Cham, ISBN 978-3-319-07271-5, doi:10.1007/978-3-319-07272-2.
4. Holmes, C., B. W. Drinkwater, and P. D. Wilcox. 2005. "Post-processing of the full matrix of ultrasonic transmit–receive array data for non-destructive evaluation," *NDT E International*, 38(8):701–711, ISSN 0963-8695, doi:https://doi.org/10.1016/j.ndteint.2005.04.002.
5. Frazier, C. and W. O'Brien. 1998. "Synthetic aperture techniques with a virtual source element," *IEEE Transactions on Ultrasonics, Ferroelectrics, and Frequency Control*, 45(1):196–207, ISSN 1525-8955, doi:10.1109/58.646925.
6. Wilcox, P., C. Clark, and B. Drinkwater. 2006. "Enhanced Defect Detection and Characterisation by Signal Processing of Ultrasonic Array Data," .
7. Yang, J., L. Luo, K. Yang, and Y. Zhang. 2020. "Ultrasonic Phased Array Sparse TFM Imaging Based on Virtual Source and Phase Coherent Weighting," *IEEE Access*, 8:185609–185618, ISSN 2169-3536, doi:10.1109/ACCESS.2020.3030246.
8. Gantala, T., S. P.L., and K. Balasubramaniam. 2023. "Improved imaging technique for non-destructive evaluation using arbitrary virtual array source aperture (AVASA)," *NDT E International*, 138:102869, ISSN 0963-8695, doi:https://doi.org/10.1016/j.ndteint.2023.102869.
9. Gantala, T., M. R. Gurunathan, and K. Balasubramaniam. 2023. "Arbitrary Virtual Array Source Aperture (AVASA) Ultrasound Imaging Technique Using Phased Array Excitation," *Journal of Nondestructive Evaluation*, 42(3):71, ISSN 1573-4862, doi:10.1007/s10921-023-00985-3.
10. P.L., S., T. Gantala, and K. Balasubramaniam. 2024. "Multi modal data fusion of PAUT with thermography assisted by Automatic Defect Recognition System (M-ADR) for NDE Applications," *NDT E International*, 143:103062, ISSN 0963-8695, doi:https://doi.org/10.1016/j.ndteint.2024.103062.